# A Self-Learning Neuromorphic System

Rory Lewis*, Michael Bihn†, Zhenqi Liu‡, Daniel S. Barbotko§
Department of Computer Science. University of Colorado at Colorado Springs
Colorado Springs, Colorado, USA
*rlewis5@uccs.edu, †mbihn@uccs.edu, ‡zliu3@uccs.edu
§dbarbotk@uccs.edu

***Abstract*—In the continuing research to implement a plurality of self-wiring synapses comprised of Field Programmable Gate Arrays (FPGAs) on a Complementary Metal Oxide Semiconductor (CMOS) system to accommodate Artificial Intelligence (AI) on a microprocessor, we delve into how a system can emulate not just a self-wiring CMOS system, but also how it can emulate brain growth at the connectome level. The enigma of contemporary advancements in AI and chip manufacturing diverging from bio-inspired systems is fascinating, especially given that AI and microprocessor engineers readily acknowledge the superior capabilities of biological brains. This paper introduces a bio-inspired device made of steel, plastic, and silica, which autonomously rewires itself, evolving and enhancing its intelligence without human intervention. The research will delve into the intricacies of the FPGA prototype's functionality, shedding light on both its technical aspects and the broader social and technological implications associated with the development of this neuromorphic chip. Next, we introduce the theoretical ability for the CMOS to grow its connectivity to FPGAs as does a human baby. Herein, we introduce the uniqueness of applying the logistical growth function to the curve fitting of the multidimensional measures of brain growth, on a CMOS system.**

***Index Terms*—Bio-Inspired; Neuromorphic; AI.**

## I. Introduction

The motivation for this research effort is that, despite significant advances in neuromorphic systems, the AI systems based on them are still far from their biological counterparts [1]. Such gaps exist because, while the world lauds the progress of ChatGPT and other high-end AI systems, the engineers are reticent to reveal that these systems consume approximately 200 terawatt hours of energy per year [2], shown in Fig. 1a. The issue is that there is no financial impetus for chipmakers to stop reaping the financial benefits of this explosion in processor requirements and take on high-risk bio-inspired chips. We will illustrate how state-of-the-art systems such as TrueNorth, Loihi, SpiNNaker, BrainScaleS, and NeuronFlow [3] have been unable to synthesize biological neurons onto a solid-state-device because: i) their neuromorphic hardware systems are based on existing CMOS technology, and CMOS devices can only numerically simulate biological neural networks [1], and ii) neuroscientists do not understand exactly how neurons function. Specifically, we do not understand how neurogenesis, differentiation, and synaptogenesis work [4]. Yes, we know that: i) neurons send and receive neurotransmitters, chemicals that carry information between brain cells [5], and ii) depending on where a neuron is located, it can perform the job of a sensory neuron, a motor neuron, or an interneuron, so there is no single process that explicitly synchronizes the work of all neurons [4]. We can show this flaw by considering the following abridged neurological developmental scenario.

**EXAMPLE 1** *First Event*: In Fig. 1b, the child is playing with his red ball. He releases it and notices that the ball dropped downwards onto the floor. We represent this by simplifying the synaptic-dendrite connections and its neuron with a green dot. We note that, for argument's sake, he also receives 100,000 sensory items with the first six being: i) he is on a soft carpet, ii) in the living room, iii) Mom is happy, vi) outside the sky is bright blue, v) birds are singing, and vi) it is nice and warm. Similarly, the last three of the 100,000 sensory item neurons are labeled 99,998 99,999 and 100,000. *Second Event*: Two weeks pass. In Fig. 1c, Mom and Dad visit a friend while the child sleeps. At the end of the evening, while Dad carries him outside and fastens him into the car seat, the child awakens and again drops his red ball. He notices that, just like two weeks ago, it dropped downwards again onto the floor of the car. It did not go up. Again, his brain receives 100,000 sensory pulses - the first six being: i) he's in a car, ii) Dad is talking on the phone, iii) Mom is not happy. iv) it is dark outside, v) it is raining and vi) it is cold. As before, we label the last three of the 100,000 sensory item neurons, 99,998 99,999 and 100,000. Note that the orange arrow in Fig. 2b represents synaptic connectivity between the *First Event* and the *Second Event*. This illustrates synaptogenesis, which is the formation of synapses between neurons in the nervous system.

### A. Synaptogenesis

The phenomena of synaptogenesis have been difficult for neuroscientists to study. Consider what happens when synaptogenesis fails: Fig. 3a represents that moment of time right before the orange arrow correctly connects synapses together. We represent this moment and illustrate failed synaptogenesis by randomly connecting *First Event* neurons with *Second Event*

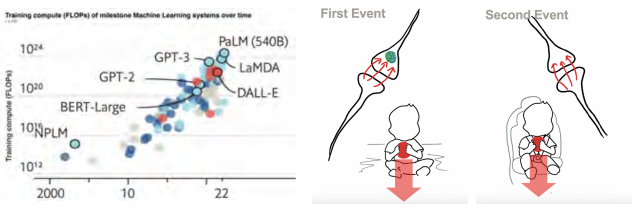


(a) (b) (c)

Fig. 1. **(a)** Increase in computing power demands petaFLOPS [6]. **(b)** Baby lets go of his red ball. **(c)** Baby lets go of his red ball again.

 ISBN: 978-1-68558-127-5 

synapses. Here, the blue synaptic connection has incorrectly connected the Living Room to the Car. If one believed this was correct and asked the child; "*Since your ball dropped when you were in the Living Room it obviously will not drop when you're in the Car, it may go to the ceiling, right*?" The child would think that was absurd. Similarly, this paper shows why present-day AI systems on both von Neuman and Neuromorphic chips are NOT autonomous. In other words, both systems still need humans to train the AI to learn. For example, Living Rooms and Cars have nothing to do with the ball dropping. It is important to remember that humans, coding the AI, would have to train the AI to learn that the *purple* line in Fig. 2a connecting *Carpet* with *Mom Not Happy* is wrong. Meaning, we would have to train our AI that *Birds Singing* with *Sound of Rain* and *100,000* with *99,998* have nothing to do with the ball dropping.

**EXAMPLE 2**. Consider a video on YouTube called "*Donkeys laughing at a Dog that Electrocutes Himself*". Fig. 4b shows that when the dog goes up to the donkeys, his nose touches an electric fence, and he is shocked. Intuitively, we know that the next time the dog passes the fence, he will not think: "*It's dark now, or there's no donkeys now, or it's raining, so now I can touch the fence*!" As absurd as this sounds, we humans have to code even the best AI systems to ignore millions of these unrelated states and synapses.

### *B. IBM's bump*

When TrueNorth engineers and neuroscientists from International Business Machines Corporation (IBM) studied how to emulate synaptogenesis, as illustrated in Fig. 2b, they assumed that the voltage inside the orange arrow was that of a typical sine wave, the fundamental waveform they'd seen many times in electroencephalograms (EEGs) and electrocardiograms (EKGs), from which other waveforms such as Gaussian curves may be generated. Here, they developed a modular approach to map bio-inspired excitatory and inhibitory conductance-based neural elements onto hardware [7] as illustrated in Fig. 3 where we see how our orange arrow connects two neurons. Here, an incoming spike signal arrives from the red horizontal axons, and is collected at the end of the orange arrow by the red vertical dendrites.

However, while Defense Advanced Research Projects Agency (DARPA) and IBM celebrated TrueNorth's ability to run at a very low rate of power, these Axon-Hillock neurons inside the orange arrow were not connecting correctly [8]. Schmidt & Avitabile found that TrueNorth's sinusoidal wave's orange arrow was randomly connecting, as illustrated in Fig.

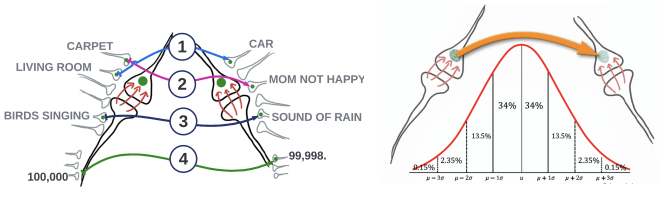


(a) (b)

Fig. 2. **(a)** FAILED Synaptogenesis. Neurons randomly connect with Second Event synapses. **(b)** IBM's assumed signal over the neuron.

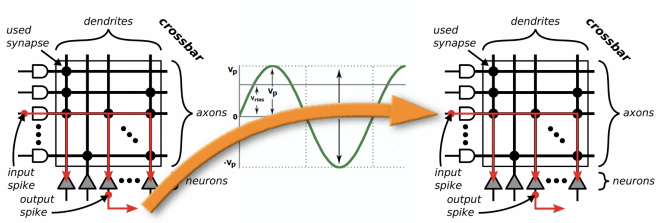


Fig. 3. Assumed signal onto spiking neuromorphic TrueNorth hardware [11].

2a, to any neuron in the fully connected layer [9]. This explains why IBM's engineers were either: i) using a huge number of cores as splitters to implement this fanout as shown in Fig. 4a or ii) adding additional hardware resources to rearrange the 3D convolutional layers [10].

### *C. Houston, IBM Has a Problem*

The authors were intrigued, and went back to Fig. 1 and asked themselves: "How does the neuronal path of the red ball neuron, illustrated by the orange arrow, know that it is going to disregard: *carpet*, *living room*, *Mom's mood*, etc. and only connect the correct dendrites?" Surely the answer must lie somewhere in the information on that neuron's sinusoidal wave, that guides it to the correct dendrite.

Going back to 1934, the studies of Hodgkin & Huxley (H&H) seemed like a great place to start reexamining the conceptual framework to understand neuromorphic spike propagation in axons and presynaptic inhibition on spike propagation. Right from the beginning, when H&H clamped an oscilloscope onto a giant squid's neurons, which are about 100 times larger than a human's neuron since they have no skull [13]–[15], the H&H research proved that dendrites are equipped with not one, but many voltages from the Ca2+ dendritic and axosomatic channels [12]. These channels proved to give rise to local spikes in dendrites and dendritic spines, as illustrated by Larkum *et al*, in Fig. 4c [13], where they examined the timing and cause of a burst from a single Na+ action potential. Here, H&H observed a biocytin-filled L5 neocortical pyramidal neuron of a rat brain using four electrodes, visible as silhouettes in Fig. 4c [16].

In 1940, Curtis & Cole [15] continued H&H's experiments

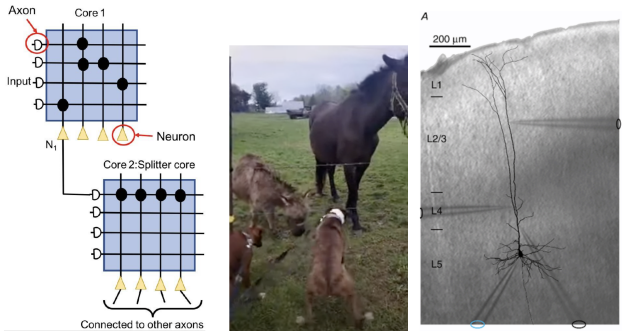


(a) (b) (c)

Fig. 4. **(a)** Splitters on TrueNorth for increasing a neuron's fan-out [9]. **(b)** Shocked. **(c)** Neocortical pyramidal neuron of rat brain [12].

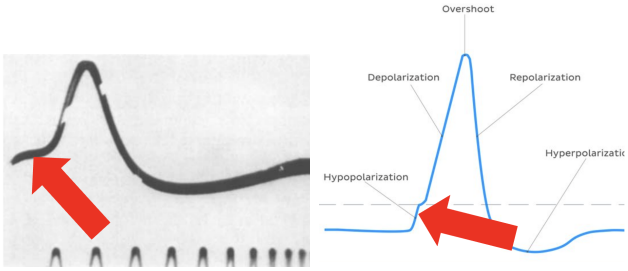


(a) (b)

Fig. 5. **(a)** Membrane potentials of the squid axon from a capillary electrode. **(b)** hypopolarization.

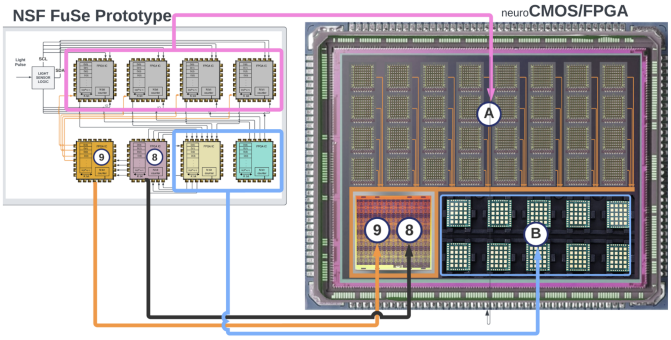


Fig. 6. Comparison of the architecture of the prototype and neuroCMOS/FPGA.

of measuring the voltage across a neuron by inserting a small electrode through the membrane of a giant squid's axon, and then into the squid's axoplasm. They found that this yielded a relatively small amount of injury to the axon. Then, they measured the potential between the inside and outside electrode, yielding the result shown in Fig. 5a. It became clear that during the three phases of the action potential (depolarization, overshot, repolarization) we do indeed witness a sinusoidal wave. However, as shown in Fig. 5b, there is a short 'hidden state' [17] of hypopolarization, which precedes the depolarization, that forms a very small bump. This, in a sense, piggy-backs on the trailing edge of the sinusoidal-biological wave, as indicated by the red arrows in Fig. 5a & b. Additionally, we note that in Fig. 7a, this addition of the same small bump ① onto the sinusoidal wave on our bio-inspired chip ②, corrects the sinusoidal wave in Fig. 2b, and was most likely overlooked by IBM's engineers.

**PRELIMINARIES** Fig. 6 illustrates how our prototype on the left side, called NSF FuSe Prototype, is being converted into our neuroCMOS/FPGA architecture on the right. The prototype's Grey State FPGAs, highlighted by the pink box, are replaced by section Ⓐ in the neuroCMOS/FPGA architecture that is comprised of 32-memristors. This means the chip can autonomously re-wire neurons (FPGAs) between 32 states, whereas our prototype only had four states. Additionally, the neuroCMOS/FPGA architecture is comprised of neuromorphic controllers based off the Linearized Hodgkin-Huxley circuits designed in 1934 [18]. Note that the FPGAs highlighted by the blue box, execute the trivial function of only allowing an input from a sensor to move to the next available memristor,

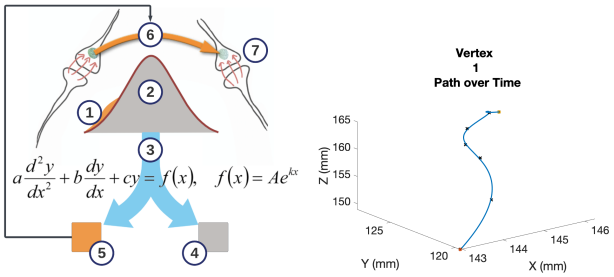


(a) (b)

Fig. 7. **(a)** 2nd Order Diff Eq conversion. **(b)** 3D graphic shows the path the first vertex takes through the brain from 1 month (pentagon) to 24 months(hexagon)

and then order it in an **n x n** sequence in the memristor itself, located in Ⓐ. The realization of this small bump, shown as ① in Fig. 7a, forms the basis for our hypothesis for this research effort. Taking the 2nd order Differential Equation ③ of both ① and ② we split the combined area under the curve into grey area ④ that constitutes the power necessary to project the neuron's signal ⑥ across the orange arrow to its destination ⑦, while the orange area ⑤ is what we believe, carries the neuron's ROAD MAP that guides it to its destination ⑦.

**THE ISSUE FOR THIS PAPER** *is that we do not know: i) how many FPGAs we will need to sort and order the data in each memristor and ii) how we need to design the neuroCMOS/FPGA architecture to expand its knowledge and neuronal connection in a way that will mimic how brains in nature grow and expand.* Additionally, to complicate the issue, the 'FPGA ⑧ & ⑨' in the neuroCMOS/FPGA architecture is not a square unit but rather a series of FPGA gates. These gates do both the matrix mathematics and the synaptogenesis of rewiring the connectors in the neuroCMOS/FPGA chip.

## II. EXPERIMENTS

### A. Hypothesis

Our hypothesis is that the optimal means to design the autonomous addition of synapses (FPGAs) is to leverage our research measuring how the human brain expands and grows connectomes in the infantile brain.

### B. Mathematically Defining Connectome Growth

To code how our neuroCMOS/FPGA will autonomously expand, we first need to mathematically define connectome growth in the infantile brain. To accomplish this, we continue our research from our last article in the BrainInfo2023 [19]. We bring in the MatLab poly5 fittings for the X, Y and Z longitudinal values of the first vertex over 1, 3, 6, 9, 12, 18 and 24 months. Using the fitted curves for the coordinates over time yields a very nice path as seen in the Fig. 7b. We use these functions to build the unit tangent vector as the directional vector for the directional derivative. Usually, the directional derivative is built with the maximized gradient on the surface, but we do not have a surface with the data from the baby connectome data. The best we can build is the unit tangent vector which we substitute in for the maximized gradient. The functions for the smoothed curves of X from "poly5" are fifth degree polynomials with coefficients: p1 =

1.742e-05, p2 = -0.001163, p3 = 0.02857, p4 = -0.3194, p5 = 1.702, p6 = 141.5. This yields a function for the x variable of the first vertex position in eq.(1).

$$X(t) = p1 * t^5 + p2 * t^4 + p3 * t^3 + p4 * t^2 + p5 * t + p6$$
$$X(t) = 1.742e-05 * t^5 + -0.001163 * t^4 + 0.02857 * t^3 + -0.3194 * t^2 + 1.702 * t + 141. \quad (1)$$

The functions for the smoothed curves of Y from "poly5" are fifth degrees polynomials with the following coefficients: p1 = -9.346e-07, p2 = 7.466e-05, p3 = -0.0008573, p4 = -0.05254, p5 = 1.396, p6 = 118.2.

Next, we used the unit tangent to find the directional derivative over 1 month to 24 months in one tenth of a month interval. This directional derivative is a better representation of the growth rate than the previously presented derivatives in each of the axis (X, Y, Z). With the first data collection at one month, the first growth rate we observe is approximately 3.46 mm. The growth rate then spikes back up to 0.482478 mm/month at 24 months of age. This same analysis can be performed on any of the 163,842 vertices tracked in the diffusion tensor magnetic resonance imaging (DT/MRI). This directional derivative could then be curve fitted to provide coefficients of growth to represent a particular vertex for a particular patient with specific traits. Using the baby connectome data from the human connectome project we have devised a method to provide coefficients of growth. These coefficients could then be used to find correlation between growth and behavioral traits. There is most likely some correlation between the coefficients and DNA. Of course, we will need long term DT/MRI data from thousands of patients over the first two years of life to obtain the big data necessary for machine learning.

### C. Logistical Growth Function Solved for $\rho$

From differential equations [20] we have the logistical growth model. Let us first review exponential growth. The rate of change of a population's growth is dependent on the current population. Here $y$ is the population and $dy/dt$ is the rate of population change over time as seen in (2). Replacing the $f(y)$ with $r$ representing the rate of growth that is proportional to the population, it yields (3).

$$\frac{\partial y}{\partial t} = f(y) \quad (2) \qquad \frac{\partial y}{\partial t} = ry \quad (3)$$

Note that for infantile brain growth we will only examine positive $r$, rate of growth. Divide both sides by $y$ and multiple both sides by $\partial t$ yields (4), then after integrating both sides we get (5) to which we take the exponential of both sides and yield (6).

$$\frac{\partial y}{y} = \frac{r}{\partial t} \quad (4) \qquad ln(y) = rt + c \quad (5) \qquad y = e^{rt+c} = e^c e^{rt} \quad (6)$$

Going to the logistic growth, we replace the $r$ with a function of $y$, $h(y) = r$. We need to choose $h$ such that when $y$ is either small or large, $h(y) > 0$ it reflects the start of growth, and limits factors of starvation. Here, $h(y) = (r - ay)$ satisfies these conditions. Applying applicable algebra in (7 & 8).

$$h(y) = r(1 - \frac{ay}{r}) \quad (7) \qquad \frac{\partial y}{\partial t} = r(1 - \frac{ay}{r})y \quad (8)$$

We let $k = \frac{a}{r}$ where $r$ is intrinsic growth rate and K becomes the equilibrium for a sustained population greater than zero. Note that we will not attain $K$ as we know the brain continues to grow after two years of age as shown in (9), and with zero growth in (10).

$$\frac{\partial y}{\partial t} = r(1 - \frac{y}{K})y \quad (9) \qquad 0 = r(1 - \frac{y}{K})y \quad (10)$$

This is satisfied when either $y = 0$ or when $(1 - \frac{y}{K})$ is zero, hence $y = K$. We know that at birth, the brain has some volume of neurons, therefore we will not consider $y = 0$ or a population of zero. Dividing both side by $(1 - \frac{y}{K})y$ and multiplying both sides by $\partial t$:

$$\frac{\partial y}{(1 - \frac{y}{K})y} = r\partial t \quad (11)$$

Perform Partial Fractions

$$\frac{1}{(1 - \frac{y}{K})y} = \frac{A}{y} + \frac{B}{(1 - \frac{y}{K})} \quad (12)$$
$$\frac{1}{(1 - \frac{y}{K})y} = \frac{A}{y} * (\frac{1 - \frac{y}{k}}{1 - \frac{y}{k}}) + \frac{B}{(1 - \frac{y}{K})} * \frac{y}{y}$$
$$A * (1 - \frac{y}{k}) + B * y = 1$$

letting $\frac{y}{k} = 1$ or $y = k$ we get $B * y = 1$, and then dividing by $y$ and substituting $k$ for $y$ we get $B = \frac{1}{k}$ and then substituting back into (13 & 14),

$$A*(1-\frac{y}{k})+\frac{y}{k} = 1 \quad (13) \qquad A = \frac{(1 - \frac{y}{k})}{(1 - \frac{y}{k})} = 1 \quad (14)$$

It yields (15) and now we integrate both sides by breaking the left side apart as seen in (16)

$$(\frac{1}{y} + \frac{\frac{1}{k}}{(1 - \frac{y}{k})})\partial y = r\partial t \quad (15) \qquad \int \frac{1}{y}\partial y = ln|y| \quad (16)$$

for (17), then using a $u$ substitution we get (18).

$$int \frac{\frac{1}{k}}{(1 - \frac{y}{k})}\partial y \quad (17) \qquad \partial u = -\frac{1}{k}\partial y \quad (18)$$

by the chain rule, with $g(x) = uf(u) = \frac{1}{u}$

$$\int f(g(x))g'(x) = \int f(u)\partial u = ln|u| = ln|1 - \frac{y}{K}|$$

therefore

$$\int (\frac{1}{y} + \frac{\frac{1}{k}}{(1 - \frac{y}{k})})\partial y = \int r\partial t \quad (19)$$

becomes

$$ln|y| - ln|1 - \frac{y}{K}| = rt + c \quad (20)$$

otherwise known as the logistical growth model.

Note that the neuron growth does not depend on the number of neurons as population growth does. Rather, neuron growth depends on the number of radial glial cells which are dependent on the number of neuroepithelial cells [21]. The number of these different cell types are unavailable at this time. Thus, our challenge is to build a logistical brain growth model that shows the dependencies on the different cell populations and to do this we move from the logistical growth function to the Reaction Diffusion Equation.

From the Mathematical Biology text [22] and Konukoglu *et al.* [23] we have:

$$\frac{\partial u}{\partial t} = \nabla \cdot (D\nabla u) + \rho u(1-u) \tag{21}$$

with $D\nabla u \cdot \vec{n}_{\rho\Omega} = 0$ Where $u$ being density, D is the Diffusion tensor, $\rho$ is the proliferation rate, $\Omega$ the brain domain, and $\rho\Omega$ the brain boundaries [23] "The traveling wave solution of Equation 21 has the form

$$u(x,t) = u(x - vt) = u(\mathcal{E}) \tag{22}$$

where $\mathcal{E}$ is the moving frame and v is the asymptotic speed of this frame, the wavefront. When this solution is plugged into the reaction-diffusion equation 21 we obtain the ordinary differential equation" known as the Eikonal Equation.

$$\mathbf{n}' D\mathbf{n}\frac{\partial^2 u}{\partial \mathcal{E}^2} + v\frac{\partial u}{\partial \mathcal{E}} + \rho u(1-u) = 0 \tag{23}$$

The Eikonal equation has been used to describe brain tumor growth [23]. Konukglu *et al.* discerned the growth rate difference of brain tumors in white matter vs. grey matter. Since DT-MRI do not provide density Konukglu *et al.* switched their parameter to the moving front of the tumor cell. With the data from the Baby Connectome Project (BCP), we have polygons (triangles) of area. We also have no diffusion data. And we see that the area of the triangles are increasing. We make the presumption that there is no diffusion. Eliminating the diffusion term from the reaction diffusion equation yields the logistical growth function (24).

$$\frac{\partial A}{\partial t} = -\rho A(1 - \frac{A}{K}) \tag{24}$$

The same result can be obtained by using the *Fisher-Kolmogoroff equation* from [24] [22] and setting the diffusion term to zero. With K(capacity) being the max surface area attained. For this work, we are only looking at the growth from 1 month to two years. The max surface area will be the surface area at two years of age. We attain $\frac{\partial A}{\partial t}$ by curve fitting the surface area over time and taking the derivative. Then we can attain $\rho$, the growth function for the area of the entity being investigated. Dividing both sides by $A\ (1 - \frac{A}{K})$

$$\frac{\frac{\partial A}{\partial t}}{A(1-\frac{A}{K})} = -\rho \tag{25}$$

$$\rho = -\frac{\frac{\partial A}{\partial t}}{A(1-\frac{A}{K})} \tag{26}$$

Thus, we have produced a differential equation $\rho(t)$ equal to the first derivative of brain surface area over time divided by a function of surface area over time. Several neuroscientists have noted that different lobes and white matter pathways develop at different times and rates. With this methodology we can construct the logistical growth functions, $\rho_i(t)$, to reflect those differences by constructing a sum of $\rho_i(t)$ where t is all the triangles of a given lobe. Brain growth is reflected by several measures, those being increasing surface area, increasing volume and vertex movement through the skull which is also growing. The grey matter has 14 layers which comprise the grey matter lobes. The 42 white matter pathways grow underneath the gray matter layers. For each of these measures, we define the characteristic to describe the individual lobe/pathway to be time dependent, hence the characteristics to be solved for are:

$$C_i(t) = \rho_i(t), \forall i = lobes, pathways \tag{27}$$

where i represents the brain lobe/pathway under consideration.

### *D. Logistical Growth Function Applied to Brain Surface Area Growth*

The polygons are actually triangles. We found the polygons are stable over time, and they have the same vertices at the seven times utilized in this work. The numbered polygons, 327,680 of them, have the same vertices, in the same order, for all seven times, 1, 3, 6, 9, 12, 18 and 24 months of age. Since the brain is growing, we expect the area of the polygons will grow over time. We use the three-dimensional distance formula to obtain the length of each of the three sides of the triangle in (28). We then use Heron's Formula [25] (28).

$$l = \sqrt{(X1 - X2)^2 + (Y1 - Y2)^2 + (Z1 - Z2)^2} \tag{28}$$

Rather than calculating the base and the height of the triangle, Heron's formula is simplistic in its three subtractions, three multiplications and one square root in (29).

$$area = \sqrt{s * (s-a) * (s-b) * (s-c)} \tag{29}$$

We examined the first polygon in the Visualization Toolkit (VTK) files. It consists of vertices 1, 40965, and 40963. Over time we found the areas were 0.0312, 0.0426, 0.0555, 0.0606, 0.0648, 0.0665, 0.0730. And yes, the area of the polygon is increasing over time. We apply curve fitting methodology for polygon 1 area. Polygon 1 consists of vertices 1, 40965, and 40963. These positions are subsequently used for the monthly area calculations. The curve fitting of the Area over time produced a piecewise solution of six equations. The first equation is used from one month to three months. The second equation is used from three months to six months and so forth. Third equation, six to nine months, forth, nine to twelve months, fifth, twelve to eighteen months, sixth, eighteen to twenty-four months. These equations were used to plot the line in Fig. 8 where each equation is of the form $a * t^3 + b * t^2 + c * t + d$ yielding the coefficients for the six equations for the resulting coefficients for the piece-wise solution to the curve fitting of actual polygon 1 area at 1, 3, 6, 9, 12, 18, and 24 months, as seen in Table I.

 ISBN: 978-1-68558-127-5 

TABLE I
COEFFICIENTS FOR THE SIX EQUATIONS

| eq # | a | b | c | d | months |
|---|---|---|---|---|---|
| 1 | -3.2754e-05 | 0 | 0.0052 | 0.0321 | 1-3 |
| 2 | -1.9036e-05 | -1.9653e-04 | 0.0048 | 0.0422 | 3-6 |
| 3 | 2.3455e-05 | -3.6785e-04 | 0.0031 | 0.0544 | 6-9 |
| 4 | 3.3306e-06 | -1.5676e-04 | 0.0016 | 0.0612 | 9-12 |
| 5 | 1.2741e-05 | -1.2678e-04 | 7.0962e-04 | 0.0645 | 12-18 |
| 6 | -5.6974e-06 | 1.0255e-04 | 5.6424e-04 | 0.0670 | 18-24 |

To build the six equations for area growth we start with the first derivative yielding growth rate. Each equation is of the form: $a*t^2+b*t+c$ yielding coefficients for the six equations as shown in Table II.

TABLE II
FIRST DERIVATIVE YIELDING GROWTH RATE

| eq # | a | b | c | months |
|---|---|---|---|---|
| 1 | 3*-3.2754e-05 | 0 | 0.0052 | 1-3 |
| 2 | 3*-1.9036e-05 | 2*-1.9653e-04 | 0.0048 | 3-6 |
| 3 | 3*2.3455e-05 | 2*-3.6785e-04 | 0.0031 | 6-9 |
| 4 | 3*3.3306e-06 | 2*-1.5676e-04 | 0.0016 | 9-12 |
| 5 | 3*1.2741e-05 | 2*-1.2678e-04 | 7.0962e-04 | 12-18 |
| 6 | 3*-5.6974e-06 | 2*1.0255e-04 | 5.6424e-04 | 18=24 |

With the function for Area over time and the first derivative for Area over time, we can now solve for $\rho$, the logistical growth function of Area over time. Using the definition of $\rho$ from the previous section we have:

$$\rho = -\frac{\frac{\partial A}{\partial t}}{A(1-\frac{A}{K})} \tag{30}$$

where $K$ is the area of the polygon at max growth in Fig. 8a.

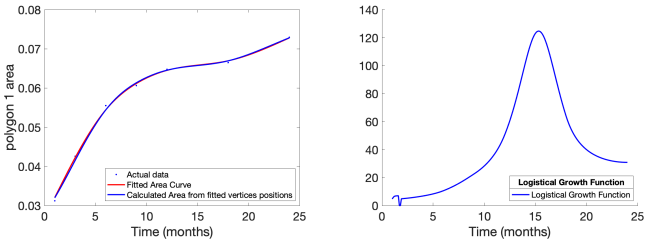


(a) (b)

Fig. 8. **(a)** The difference between the actual areas (points) and fitted curve for area and the calculated area from the fitted vertices over time. **(b)** The Logistical growth function for the polygon 1 area of the brain from one month to twenty-four months of age.

## III. CONCLUSION & FUTURE WORK

Because our neuroCMOS/FPGA is in an "*infantile*" state, we barely have to go beyond the infantile state for a human. Here we have concluded that, with this statement in mind, we can set $K$ to a number greater than the area obtained at two years of age, avoiding the divide by zero anomaly. We currently set $K$ to twice the polygon 1 area at two years of age and plot this logistical growth function from one month to twenty-four months as shown in Fig. 8b. Next, we model the aforementioned onto a simulated software version of our neuroCMOS/FPGA, that will show we can procure a chip that rewires itself and grows like an infantile's brain grows.

## REFERENCES

[1] D. Ivanov, A. Chezhegov, M. Kiselev, A. Grunin, and D. Larionov, "Neuromorphic artificial intelligence systems," *Frontiers in Neuroscience*, vol. 16, p. 1513, 2022.

[2] A. Mehonic and A. J. Kenyon, "Brain-inspired computing needs a master plan," *Nature*, vol. 604, no. 7905, pp. 255–260, 2022.

[3] P. Pietrzak, S. Szczęsny, D. Huderek, and Ł. Przyborowski, "Overview of spiking neural network learning approaches and their computational complexities," *Sensors*, vol. 23, no. 6, p. 3037, 2023.

[4] "Brain basics: The life and death of a neuron," 2019, [Online; accessed 2024-01-24]. [Online]. Available: https://www.ninds.nih.gov/health-information/public-education/brain-basics/brain-basics-life-and-death-neuron

[5] N. Banerjee, "Neurotransmitters in alcoholism: A review of neurobiological and genetic studies," *Indian journal of human genetics*, vol. 20, no. 1, p. 20, 2014.

[6] C. Szegedy *et al.*, "Intriguing properties of neural networks," *arXiv preprint arXiv:1312.6199*, 2013.

[7] M. P. Löhr, C. Jarvers, and H. Neumann, "Complex neuron dynamics on the ibm truenorth neurosynaptic system," in *2020 2nd IEEE International Conference on Artificial Intelligence Circuits and Systems (AICAS)*. IEEE, 2020, pp. 113–117.

[8] R. A. Nawrocki, R. M. Voyles, and S. E. Shaheen, "A mini review of neuromorphic architectures and implementations," *IEEE Transactions on Electron Devices*, vol. 63, no. 10, pp. 3819–3829, 2016.

[9] H. Schmidt and D. Avitabile, "Bumps and oscillons in networks of spiking neurons," *Chaos: An Interdisciplinary Journal of Nonlinear Science*, vol. 30, no. 3, 2020.

[10] R. Shukla, M. Lipasti, B. Van Essen, A. Moody, and N. Maruyama, "Remodel: Rethinking deep cnn models to detect and count on a neurosynaptic system," *Frontiers in neuroscience*, vol. 13, p. 4, 2019.

[11] P. R. Huttenlocher and A. S. Dabholkar, "Regional differences in synaptogenesis in human cerebral cortex," *Journal of comparative Neurology*, vol. 387, no. 2, pp. 167–178, 1997.

[12] Y. Manor, J. Rinzel, I. Segev, and Y. Yarom, "Low-amplitude oscillations in the inferior olive: a model based on electrical coupling of neurons with heterogeneous channel densities," *Journal of neurophysiology*, vol. 77, no. 5, pp. 2736–2752, 1997.

[13] C. Meunier and I. Segev, "Playing the devil's advocate: Is the hodgkin–huxley model useful?" *TRENDS in Neurosciences*, vol. 25, no. 11, pp. 558–563, 2002.

[14] B. L. d'Incamps, C. Meunier, D. Zytnicki, and L. Jami, "Flexible processing of sensory information induced by axo-axonic synapses on afferent fibers," *Journal of Physiology-Paris*, vol. 93, no. 4, pp. 369–377, 1999.

[15] H. J. Curtis and K. S. Cole, "Membrane action potentials from the squid giant axon," *Journal of Cellular and Comparative Physiology*, vol. 15, no. 2, pp. 147–157, 1940.

[16] M. E. Larkum, J. J. Zhu, and B. Sakmann, "Dendritic mechanisms underlying the coupling of the dendritic with the axonal action potential initiation zone of adult rat layer 5 pyramidal neurons," *The Journal of physiology*, vol. 533, no. 2, pp. 447–466, 2001.

[17] "Action potential," [Online; accessed 2024-01-24]. [Online]. Available: https://www.kenhub.com/en/library/anatomy/action-potential

[18] L. Ribar and R. Sepulchre, "Neuromorphic control: Designing multiscale mixed-feedback systems," *IEEE Control Systems Magazine*, vol. 41, no. 6, pp. 34–63, 2021.

[19] M. Bihn and R. Lewis, "A postulate: Connectome development is the driving factor of brain growth," pp. 12–15, 2023, [Online; accessed 2024-01-24]. [Online]. Available: https://shorturl.at/IOWZ7

[20] W. E. Boyce and R. C. DiPrima, *Elementary differential equations and boundary value problems*. Wiley, 2020.

[21] M. Götz and W. B. Huttner, "The cell biology of neurogenesis," *Nature reviews Molecular cell biology*, vol. 6, no. 10, pp. 777–788, 2005.

[22] J. D. Murray, "Vignettes from the field of mathematical biology: the application of mathematics to biology and medicine," *Interface Focus*, vol. 2, no. 4, pp. 397–406, 2012.

[23] E. Konukoglu *et al.*, "Image guided personalization of reaction-diffusion type tumor growth models using modified anisotropic eikonal equations," *IEEE transactions on medical imaging*, vol. 29, no. 1, pp. 77–95, 2009.

[24] J. D. Murray, "Mathematical biology ii: Spatial models and biomedical applications," *Monographs on Applied and Computational Mathematics*, vol. 3, pp. 399–400,439, 1973.

[25] R. B. Nelsen, "Heron's formula via proofs without words," *The College Mathematics Journal*, vol. 32, no. 4, p. 290, 2001.

 ISBN: 978-1-68558-127-5 